Extension of the Viscous Collision Limiting Direct Simulation Monte Carlo Technique to Multiple Species

Derek S. Liechty[1, a)] and Jonathan M. Burt[2, b)]

[1]*NASA Langley Research Center, Aerothermodynamics Branch, MS 408A, Hampton, VA 23681*
[2]*U.S. Air Force Research Laboratory, Wright-Patterson Air Force Base, OH 45433*

[a)]Corresponding author: Derek.S.Liechty@nasa.gov
[b)]Jonathan.M.Burt@nasa.gov

Abstract. There are many flows fields that span a wide range of length scales where regions of both rarefied and continuum flow exist and neither direct simulation Monte Carlo (DSMC) nor computational fluid dynamics (CFD) provide the appropriate solution everywhere. Recently, a new viscous collision limited (VCL) DSMC technique was proposed to incorporate effects of physical diffusion into collision limiter calculations to make the low Knudsen number regime normally limited to CFD more tractable for an all-particle technique. This original work had been derived for a single-species gas. The current work extends the VCL-DSMC technique to gases with multiple species. Similar derivations were performed to equate numerical and physical transport coefficients. However, a more rigorous treatment of determining the mixture viscosity is applied. In the original work, consideration was given to internal energy non-equilibrium, and this is also extended in the current work to chemical non-equilibrium.

INTRODUCTION

Solving hypersonic reentry flows at all conditions along the trajectory of a vehicle continues to be a challenging problem. A wide range of length scales are possible where regions of both rarefied and continuum flow coexist where neither direct simulation Monte Carlo (DSMC)[1] nor computational fluid dynamics (CFD) are appropriate everywhere. Large gradient-based Knudsen values can be found within the bow shock, in the shock layer around sharp leading edges, in shock-wave/boundary-layer interaction regions, and in near-wake regions involving rapid expansion and/or comparatively low density. For flows such as these, hybrid one- or two-way coupled CFD-DSMC techniques have been developed[2-4] that can provide both high accuracy and high efficiency but tend to suffer from considerable code complexity and/or a "person in the loop" requirement, which limits automation and increases the time required to generate results. To overcome these limitations, efforts have also been devoted to the efficient extension of DSMC to very low Knudsen regimes[5, 6].

Recently, a new viscous collision limiter (VCL) DSMC technique[7, 8] has been proposed to incorporate effects of physical diffusion into collision limiter calculations. Local time step adaptation was used to equate numerical and physical transport coefficients, and a temperature-based viscosity model was employed as an alternative to collision dynamics models traditionally used for diffusive transport modeling in DSMC. The original work was derived for a single-species gas. The purpose of the current work is to extend the VCL-DSMC technique to gases with multiple, chemically-reacting species. The next sections outline updates to the VCL-DSMC technique, followed by sections where the new techniques are applied to zero-dimensional relaxation tests and a blunt body hypersonic flow.

VCL-DSMC PROCEDURES

Burt[8] originally performed a simplified analysis of artificial viscosity in collision limited DSMC calculations for simple gases. He utilized the results of that analysis to derive an expression for the local time step interval that equated artificial viscosity to a desired temperature-based dynamic viscosity. As the basis for the proposed scheme, the flow

conditions of interest were restricted to small but finite Knudsen numbers, where the velocity distribution could be described as a small perturbation from the equilibrium limit. A first order Chapman-Enskog distribution could then be substituted into the governing Boltzmann Equation. The analysis involved the direct calculation of viscosity under small Knudsen number conditions for a simple gas. Thermal conductivity was discussed, and mass diffusion coefficients were not considered. The analysis is extended in this work to gas mixtures and, although mass diffusion is important for gas mixtures and reacting-flow simulations, they are neglected in the current analysis and will be revisited in future studies.

Determination of Time Step Interval to Match Artificial and Physical Viscosities

In earlier work[8] it was proposed that the artificial viscosity in a collision limited DSMC calculation can be divided into independent contributions associated with finite collision separation and free molecular particle movement operations. For the special case of a collision limited DSMC implementation employing near/nearest neighbor collision partner selection (e.g., transient adaptive subcells or virtual subcells) along with dynamic local time step adaptation, both artificial viscosity contributions may be varied through adjustment to the local time step interval. Thus, by equating artificial and physical viscosities in each cell, we can approximately include viscous transport capabilities while maintaining the efficiency advantages of collision limited DSMC. The resulting time step interval for a two-dimensional simulation is derived as

$$\Delta t_{visc} = \frac{2}{P}\left(\mu(T) - C\rho\frac{\Lambda^2}{\Delta t_{old}} \right) \tag{1}$$

where Δt_{visc} is the resulting time step interval, P is the pressure, μ is the viscosity, T is the temperature, C is a constant (found to be approximately equal to 0.9 in previous studies), ρ is the density, Λ is the mean collision separation, and Δt_{old} is the previous time step. Of the previous variables in Eq. (1), P, T, ρ and Λ are computed as time-averaged cell quantities over a period during which the time step interval Δt_{old} was assigned.

To determine the dynamic viscosity in Eq. (1), a power law dependence was assumed between μ and the time-averaged translational temperature T according to the variable hard sphere (VHS) collision model of Bird[9]

$$\mu(T) = \frac{15\sqrt{\pi m k T_{ref}}}{2\pi d_{ref}^2 (5-2\omega)(7-2\omega)}\left(\frac{T}{T_{ref}} \right)^{\omega} \tag{2}$$

However, a more rigorous treatment of determining the mixture dynamic viscosity is required when considering a gas mixture as opposed to a simple gas. Stephani, Goldstein and Varghese[10] have developed a consistent treatment of transport properties for DSMC/CFD applications. They derive the mixture viscosity from the VHS/VSS cross-section models determined from the first-order Chapman-Enskog approximation of the mixture viscosity

$$[\mu]_1 = \sum_s b_s \tag{3}$$

where b_s is the contribution of each species to the overall mixture viscosity and is determined by solving the following system

$$\chi_s = b_s\left\{ \frac{\chi_s}{[\mu_s]_1} + \sum_{t\neq s}\frac{3\chi_t}{(\rho_s' + \rho_t')D_{st}}\left(\frac{2}{3} + \frac{m_t}{m_s}A_{st} \right) \right\} - \chi_s \sum_{t\neq s}\frac{3b_t}{(\rho_s' + \rho_t')D_{st}}\left(\frac{2}{3} - A_{st} \right) \tag{4}$$

where χ_s is the mole fraction of species s. The densities ρ_s', ρ_t' refer to the density of species (s,t) when pure at the pressure and temperature of the gas mixture. The masses m_s, m_t are the molecular masses of species (s,t). The values of μ_s, D_{st}, and A_{st} are defined as

$$[\mu_s]_1 = \frac{5k_bT}{8\Omega_1^2(2)}, \quad D_{st} = \frac{3k_bT}{16nm_{st}^*\Omega_{st}^1(1)}, \quad A_{st} = \frac{\Omega_{st}^2(2)}{5\Omega_{st}^1(1)} \tag{5}$$

where k_b is Boltzmann's constant, n and T are the number density and temperature, respectively, and m_{st}^* is the reduced mass. Finally, the collision integrals involved in computing the above is expressed in terms of the VHS parameters as

$$\Omega_{st}^{1}(1)\Big|_{VHS} = \frac{\pi}{2} d_{ref}^{2} \left(\frac{k_b T}{2\pi m_{st}^{*}} \right)^{1/2} \left(\frac{T}{T_{ref}} \right)^{\omega - 1/2} \left[\frac{\Gamma(7/2 - \omega)}{\Gamma(5/2 - \omega)} \right] \tag{6}$$

$$\Omega_{st}^{2}(2)\Big|_{VHS} = \frac{\pi}{3} d_{ref}^{2} \left(\frac{k_b T}{2\pi m_{st}^{*}} \right)^{1/2} \left(\frac{T}{T_{ref}} \right)^{\omega - 1/2} \left[\frac{\Gamma(9/2 - \omega)}{\Gamma(5/2 - \omega)} \right] \tag{7}$$

and for the VSS collision model as

$$\Omega_{st}^{1}(1)\Big|_{VSS} = \left(\frac{2}{\alpha + 1} \right) \Omega_{st}^{1}(1)\Big|_{VHS}, \quad \Omega_{st}^{2}(2)\Big|_{VSS} = \left[\frac{4\alpha}{(\alpha + 1)(\alpha + 2)} \right] \Omega_{st}^{2}(2)\Big|_{VHS} \tag{8}$$

The collision integral $\Omega_1^2(2)$ is of the form given in Eq. (6) or (8) with s=t, and Γ(x) is the gamma function.

Internal Energy Nonequilibrium

In the current model, translational nonequilibrium cannot be accurately represented. However, as discussed previously[8], internal energy nonequilibrium can be incorporated through the use of an inelastic collision probability correction. The probability of internal-translational energy exchange for a given binary collision can be calculated by expressing the number of particles N_{int}^{s} in a cell that experience internal-translational energy exchange over time Δt in two different ways. First, N_{int}^{s} is given as a function of the number of particles N_{tot} (of which N_s are of species s in the cell), the probability of energy exchange ϕ_{int}^{DSMC} (which is generally taken as the reciprocal of the collision number Z_{int} for a constant exchange probability), and the equilibrium mean collision frequency for species s, F_{coll}^{s}, which is in turn computed as a function of the cell-averaged translational temperature T

$$N_{\text{int}}^{s} = N_s F_{coll}^{s}(T) \phi_{\text{int}}^{DSMC}(T) \Delta t \tag{9}$$

Secondly, N_{int}^{s} is given as a function of the number of particles of species s that are selected to collide, N_{sel}^{s}, during the current time step, along with the probability $\phi_{\text{int}}^{VCL-DSMC}$ that any colliding particle will be selected for internal-translational energy exchange

$$N_{\text{int}}^{s} = N_{sel}^{s} \phi_{\text{int}}^{VCL-DSMC} \tag{10}$$

where the number of particles of species s participating in the collisions is found to be

$$N_{sel}^{s} = N_{coll} \frac{2N_s}{N_{tot}} \tag{11}$$

This is because, in each of the N_{coll} collisions, the probability of choosing a particle of species s randomly in the cell is N_s / N_{tot}, and then the probability that the nearest neighbor is of species s is taken to be the same. Equating the right hand sides of Eqs. (9) and (10) and solving for the new probability results in

$$\phi_{\text{int}}^{VCL-DSMC} = \frac{N_s F_{coll}^{s}(T) \Delta t}{N_{sel}^{s}} \phi_{\text{int}}^{DSMC}(T) \tag{12}$$

which is the corrected internal energy relaxation probability to be used in the VCL-DSMC algorithm, and works for rotational, vibrational, and electronic energy modes.

Chemical Nonequilibrium

Finding the corrected probability of the occurrence of a chemical reaction is similar to that of the corrected probability of internal energy exchange, but with a few different terms used. The probability of a chemical reaction, $A + B \rightleftharpoons C + D$, can be calculated by expressing the number of reactions N_{react}^{r} in a cell over time Δt for a reaction r in two different ways. First, N_{react}^{r} is given as a function of the rate of change of one of the reactants, dN_A/dt, where dN_A is the number of particles of species A in the cell that undergo the aforementioned chemical reaction

$$N_{react}^{r} = \frac{dN_A}{dt}\Delta t \tag{13}$$

where the time rate of depletion of species A can be found as

$$\frac{dN_A}{dt} = k_f(T) N_A N_B \left(W_{ref} \Big/ V \right) \tag{14}$$

where k_f is the rate constant for the reaction as a function of temperature, W_{ref} is the number of real particles per simulated particle, and V is the volume of the cell. Secondly, N_{react}^{r} is given as a function of the number of collisions performed, N_{coll}, the probability of selecting a pair of A and B particles, P^{A+B}, and the fraction of collisions that have sufficient energy to occur, F_ε

$$N_{react}^{r} = N_{coll} P^{A+B} F_\varepsilon \phi_{react}^{VCL-DSMC} \tag{15}$$

where the middle two terms on the right hand side of Eq. (16) are defined as

$$P^{A+B} = \begin{cases} \dfrac{{}^{N_A}C_1 \, {}^{N_B}C_1}{{}^{N_{tot}}C_2}, A \neq B \\ \dfrac{{}^{N_A}C_2}{{}^{N_{tot}}C_2}, A = B \end{cases}, \quad F_\varepsilon = Q\left(\bar{\zeta} + 5/2 - \omega_{AB}, \varepsilon_0 \Big/ kT \right) \tag{16}$$

where $\bar{\zeta}$ is the average number of internal degrees of freedom that participate in the reaction, ω_{AB} is the VHS viscosity index, ε_0 is the threshold energy for the reaction, k is Boltzmann's constant. The notation introduced in Eq. (17) is the number of combinations defined as

$${}^{n}C_k = \frac{n!}{k!(n-k)!} \tag{17}$$

resulting in the probability of a reaction occurring for collisions of sufficient energy

$$\phi_{react}^{VCL-DSMC} = \frac{\dfrac{dN_A}{dt}\Delta t}{N_{coll} P^{A+B} F_\varepsilon} \tag{18}$$

ZERO-DIMENSIONAL RELAXATION

The first step in demonstrating the applicability of the proposed techniques is to perform several zero-dimensional simulations and compare measured values to theoretical expectations. The first simulations are the vibrational relaxation of molecular oxygen initially at $T_{trans} = T_{rot} = 10000$ K, $T_{vib} = 0$ K, and at a number density of 1e22 m^{-3}. The O_2 had a diameter of 4.07×10^{-10} m, the reference temperature was 273 K, and the VHS viscosity index was 0.77. This test case was chosen to compare to that performed by Bird[11] where he set the vibrational collision number to a constant value of 200 and the rotational collision number to a constant value of 1. Figure 1 shows the comparison of the two techniques. The translational and rotational temperature remain essentially equal due to the fast relaxation of the rotational mode (rotational temperature is not included for clarity), and the system came to equilibrium at a temperature of 7450 K (the system moved from 5 to 6.712 degrees of freedom during relaxation - $\zeta_{vib} = 1.712$ at 7450 K). Also, the difference between the average of the translational and rotational temperatures and the vibrational temperature should fall to $1/e$ of the initial temperature of 10000 K at 200 mean collision times. The difference in temperatures reaches $10000/e$ at 206 mean collision times for the "no limiter" simulation and 240 for the VCL-DSMC simulation, so the VCL-DSMC relaxation lags behind the "no limiter" slightly.

The next simulations measure the chemical reaction rates of a five-species air system at 6000 K. This temperature was chosen to correspond to the shock layer temperatures experienced by the gas in the blunt body simulations presented in the following section. Although a total of 34 reactions are included, only a representative selection will be discussed for brevity. Probably the most significant reaction to be considered below is the dissociation of O_2 when colliding with N_2 ($O_2 + N_2 \rightleftharpoons O + O + N_2$). The Arrhenius rate coefficients used for this reaction were a = 3.321x10^{-9} and b = -1.5 with an activation energy E_a = 8.215x10^{-19} J to get the rate k_f in units of m^3/molecule/s. The expected rate at 6000 K is 3.5255x10^{-19} m^3/molecule/s. The sampled DSMC and VCL values were 3.9832x10^{-19} and 3.9263x10^{-19} m^3/molecule/s, respectively, resulting in values 13% and 11% higher than the Arrhenius value. However, according to Gimelshein[12], this is an expected result when the Arrhenius coefficients are not adjusted to account for the use of discrete internal energy modes (which was not performed for the current simulation). Another example reaction is the exchange reaction $N_2 + O \rightleftharpoons NO + N$, which is the primary path for the creation of NO. The Arrhenius rate coefficients used for this reaction were a = 9.963x10^{-17} and b = 0.1 with an activation energy E_a = 5.247x10^{-19} J to get the rate k_f in units of m^3/molecule/s. The expected rate at 6000 K is 4.2208x10^{-19} m^3/molecule/s. The sampled DSMC and VCL values were 4.6463x10^{-19} and 4.5375x10^{-19} m^3/molecule/s, respectively, resulting in values 10% and 7.5% higher than the expected value. Given the expectation of higher rates than given by the Arrhenius equation, the sampled reaction rates compare well to each other.

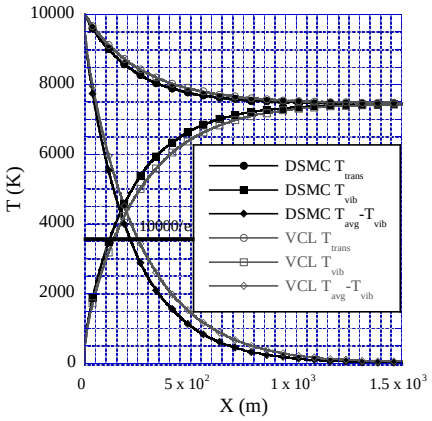

FIGURE 1. Vibrational relaxation of O_2 initially at $T_{tr} = T_{rot}$ = 10000 K, T_{vib} = 0 K with Z_{vib} = 200.

APPLICATION TO HYPERSONIC BLUNT BODY FLOW

The blunted wedge test case previously presented by Burt[8] is used again to evaluate the extensions to the VCL-DSMC technique presented in this paper. The numerical procedures discussed by Burt[8] and those presented above have been implemented in the MAP[13] DSMC code for simulation of laminar two-dimensional steady-state flows involving multiple species with negligible rarefaction effects. This test case is a two-dimensional hypersonic flow of air (23.72% O_2 and 76.28% N_2) around a blunted 30° wedge with a constant nose curvature of 5 mm. The wall is an isothermal diffusely-reflecting surface at a temperature of 800 K. The inflow properties include a temperature of 264 K, a bulk velocity of 3656.4 m/s, and a number density of 4.13e22 m^{-3}, resulting in a Mach number of approximately 11 and a global Knudsen number of 0.004. All VHS molecular properties were taken from Swaminathan-Gopalan[14] with values of Z_{rot} = 1 and Z_{vib} = 50 used for the molecular species. Free stream molar fractions were 0.2372 for O_2 and 0.7628 for N_2. A collisional equilibration length coefficient of C = 0.9 is used as determined previously and approximately 4 collisions per particle per time step occur to ensure that the velocity distribution function in each cell is fully equilibrated during collision operations. For comparison, additional "no limiter" simulations are performed using traditional DSMC procedures.

Internal Energy Relaxation

The first test case includes only internal energy relaxation without chemical reactions. Figure 2 shows the flow field translational temperature from the "no limiter" DSMC simulation. This figure represents the general flow field features and body geometry of the test cases. Observed features include a large temperature spike at the shock, as well as comparatively low temperatures within a broad post-shock expansion region and a thin boundary layer along the wall. In Fig. 3, contours are plotted for the maximum gradient length local Knudsen number Kn_{max} based on density, translational temperature, and bulk velocity based on the results of the "no limiter" simulation. This parameter is defined as

$$Kn_{\max} = \max\left\{\frac{\lambda}{\rho}|\nabla\rho|, \frac{\lambda}{T}|\nabla T|, \frac{\lambda}{a}|\nabla c|\right\} \tag{19}$$

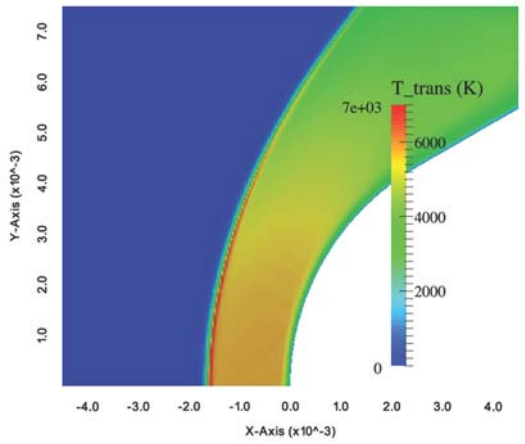

FIGURE 2. Translational temperature contours from "no limiter" DSMC simulation with no chemical reactions.

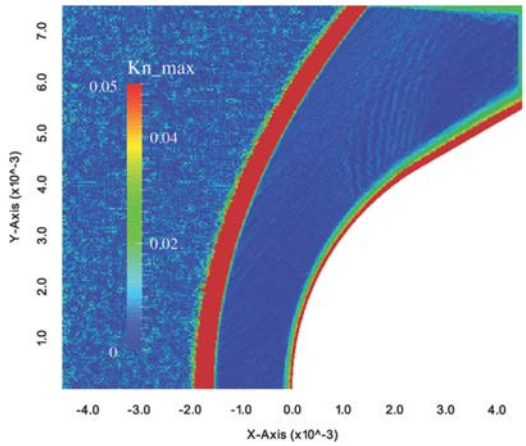

FIGURE 3. Contours of maximum gradient length local Knudsen number from "no limiter" DSMC simulation.

where λ is the local mean free path, a is the local speed of sound, and $c = \sqrt{U^2 + V^2}$ is the bulk velocity magnitude. A gradient-based local Knudsen number is often used to assess continuum breakdown, and it is often assumed that the continuum assumptions underlying the Navier-Stokes equations are invalid when $Kn_{max} > 0.05$. As shown in Fig. 3, continuum breakdown likely occurs in a region surrounding the shock, as well as a thin layer near the wall.

Continuum flow approximations behind the analysis previously[8] presented are assumed to limit the valid Kn range for VCL-DSMC procedures in a similar manner to the Navier-Stokes equations. It follows that the VCL-DSMC results in regions of significant continuum breakdown, such as the region surrounding the shock and near the wall, cannot be assumed to be accurate. This result was clearly shown in earlier work where a small discrepancy in shock standoff distance was observed and was attributed in part to the expected VCL-DSMC inaccuracy associated with continuum breakdown. Future work will focus on defining these regions of continuum breakdown and traditional DSMC simulations can then be performed in these regions.

In Fig. 4, VCL-DSMC and "no-limiter" simulation results are presented for translational, rotational, and vibrational temperatures along the stagnation line. The shaded regions indicate continuum breakdown regions according to the simple definition in Eq. (20). However, there appears to be a slightly wider region of non-continuum flow that is not captured. Recent work by Swaminanthan-Goplan, et al.,[15] indicates that an expanded definition of breakdown parameters, termed the generalized Chapman-Enskog continuum breakdown parameters, are more appropriate for defining these regions. Included are measures for multi-component diffusion, thermal diffusion, normal and shear stresses, Fourier-type heat fluxes based on translational, rotational and vibrational temperatures, bulk viscosity and relaxation pressure for chemically reacting flows. These factors were shown to characterize a much wider region of non-equilibrium than indicated by Eq. (20). However, the temperatures in the region upstream of the shock non-equilibrium region compares well, as well as most of the area between the two breakdown regions. A greater degree of nonequilibrium is expected in the current study as compared to the previous test case due to an increased free stream Mach number (11 vs. 5).

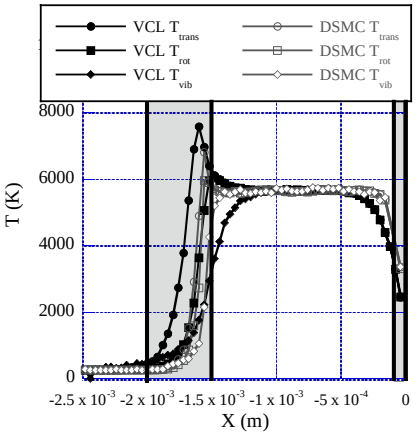

FIGURE 4. Comparison of temperatures along stagnation streamline from blunted wedge flow simulations without chemical reactions.

Chemical Nonequilibrium

The second test case is the blunt cone configuration from the previous section with internal energy and chemical reactions included. The flow field and resultant maximum gradient length local Knudsen number are similar to those presented in Figs. 2 and 3 and will not be repeated for this test case. In Fig. 5, VCL-DSMC and "no-limiter"

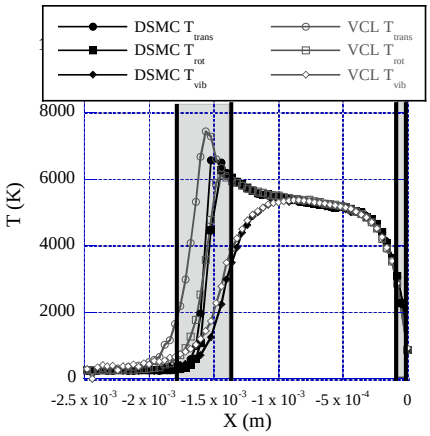

FIGURE 5. Comparison of temperatures along stagnation streamline from blunted wedge flow simulations with chemical reactions included.

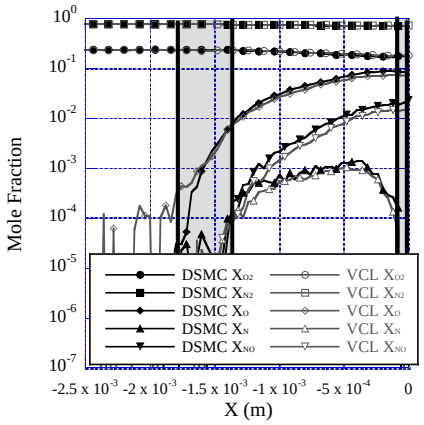

FIGURE 6. Comparison of mole fractions along the stagnation streamline from the blunted wedge flow simulations

simulation results are presented for translational, rotational, and vibrational temperatures along the stagnation streamline. The general trends are similar to the results of the blunt cone test case above without chemical reactions and the agreement is similar, as well. Just like the results from Fig. 4, the VCL-DSMC simulation is not capturing the translational non-equilibrium, as expected.

The resultant species mole fractions for the VCL-DSMC and traditional DSMC simulations are presented in Fig. 6. Again, the agreement between the two simulations is quite good, with the VCL-DSMC mole fractions slightly lower than the "non-limiter" results. In the next section, a hybrid simulation will be performed in an attempt to improve the comparisons between the fully traditional DSMC simulation and the hybrid VCL-DSMC simulation.

Hybrid Simulation

In the above simulations, it was demonstrated that the non-continuum regions of flow resulted in poor comparisons between the VCL-DSMC and traditional DSMC simulations. In an attempt to improve this discrepancy, hybrid simulations were performed where the regions of significant continuum breakdown ($Kn_{max} > 0.05$) are assigned the traditional DSMC algorithm, while regions of continuum flow are assigned the proposed VCL-DSMC algorithm.

Figures 7 and 8 present the comparison of temperatures and mole fractions, respectively, along the stagnation streamline between the hybrid simulation and traditional DSMC simulation. The initial temperature comparison is greatly improved through the shock, with the hybrid simulation resulting in a slightly thicker shock layer. There may be several reasons for the remaining differences. First, as mentioned above, we are likely not capturing the breakdown regions associated with diffusion and chemical processes. Also, as discussed by Burt[8], other possible contributing error sources include the assumption that a characteristic collisional equilibration length is exactly proportional to the mean collision separation, a lack of explicit consideration for the thermal conductivity and diffusion, and inaccuracy in advective transport calculations associated with free molecular particle streaming.

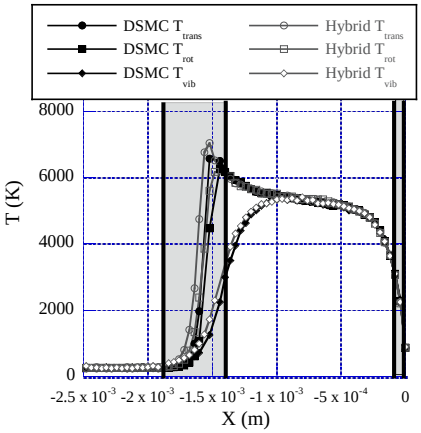

FIGURE 7. Comparison of temperatures along stagnation streamline from hybrid blunted wedge flow simulations with chemical reactions included.

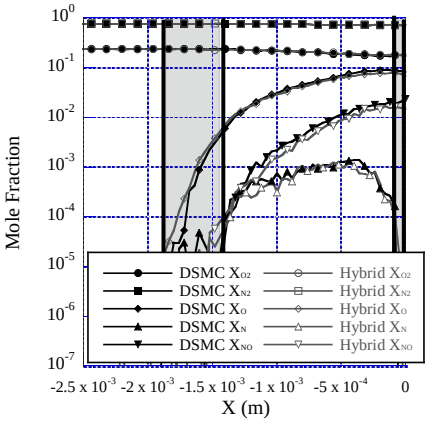

FIGURE 8. Comparison of mole fractions along the stagnation streamline from the hybrid blunted wedge flow simulations.

CONCLUSION

Modifications of the DSMC collision limiter concept, known as the viscous collision limited (VCL) DSMC technique, have been proposed as a means of efficiently applying DSMC procedures to low-*Kn* laminar steady-state gas flows with significant viscous effects. The current paper expands the original work from a simple gas technique to one incorporating multiple, chemically reacting species. Comparisons have been performed between VCL-DSMC and traditional DSMC simulations for zero-dimensional simulations and a Mach 11 blunted wedge flow. The zero-dimensional simulations showed overall good agreement for internal relaxation and chemical reaction rates between DSMC and VCL simulations. For the blunted cone simulations, agreement between the two techniques was generally very good in regions of continuum flow. However, in the regions of non-continuum flow surrounding the shock and near the wall, agreement was not as favorable. This discrepancy was expected due to VCL-DSMC inaccuracy associated with continuum breakdown. Hybrid simulations greatly improved the prediction of temperatures through the shock.

The work presented in this paper represents an initial attempt at including multiple species and chemistry into the VCL-DSMC technique. Future efforts will be focused on refining the hybrid implementation of the VCL-DSMC and traditional DSMC techniques where the traditional algorithms will be used in regions of non-continuum flow. Particular attention will be focused on including more sophisticated methods of identifying regions of continuum breakdown and extending the technique to three-dimensional flows. The VCL-DSMC technique was developed as an alternative to the more complicated CFD-DSMC hybrid schemes for use in the simulation of mixed rarefied/continuum flows. While it is a promising hybrid scheme, further evaluations are required to determine where the VCL-DSMC technique and more traditional CFD-DSMC hybrid schemes are more appropriate.

REFERENCES

1. G. A. Bird, *Molecular Dynamics and the Direct Simulation of Gas Flows*. (Oxford University Press, Oxford, UK, 1994).
2. D. B. VanGilder, C. C. Chartrand, J. Papp, R. G. Wilmoth and N. Sinha, (AIAA Paper 2007-5704, 2007).
3. W. Wang and I. D. Boyd, (AIAA Paper 2003-3644, 2003).
4. T. E. Schwartzentruber and I. D. Boyd, Journal of Computational Physics **225**, 1159-1174 (2007).
5. J. M. Burt and I. D. Boyd, Journal of Computational Physics **228**, 460-475 (2009).
6. M. N. Macrossan and X. Geng, presented at the Rarefied Gas Dynamics: 25th International Symposium, St. Petersburg, Russia, 2007 (unpublished).
7. J. M. Burt and E. Josyula, (AIAA Paper 2014-697, 2014).
8. J. M. Burt and E. Josyula, (AIAA Paper No. 2014-2544, 2014).
9. G. A. Bird, in *AIAA Progress in Astronautics and Aeronautics: Rarefied Gas Dynamics*, edited by S. S. Fisher (AIAA, New York, 1981), Vol. 74, Part I, pp. 239-255.
10. K. A. Stephani, D. B. Goldstein and P. L. Varghese, Physics of Fluids **24** (7) (2012).
11. G. A. Bird, (CreateSpace, Charleston, 2013).
12. S. F. Gimelshein, N. E. Gimelshein, D. A. Levin, M. S. Ivanov and I. J. Wysong, Physics of Fluids **16** (7), 2442-2451 (2004).
13. D. S. Liechty, Journal of Spacecraft and Rockets **52**, 1521-1529 (2015).
14. K. Swaminathan-Goplan, University of Illinois at Urbana-Champaign, 2015.
15. K. Swaminathan-Goplan, S. Subramaniam and K. A. Stephani, (Personal Communication, 2016).